Activity of Platinum/Carbon and Palladium/Carbon Catalysts Promoted by Ni$_2$P in Direct Ethanol Fuel Cells

Guoqiang Li,[a] Ligang Feng,*[b] Jinfa Chang,[a] Björn Wickman,[b] Henrik Grönbeck,[b] Changpeng Liu,[a] and Wei Xing*[a]

Ethanol is an alternative fuel for direct alcohol fuel cells, in which the electrode materials are commonly based on Pt or Pd. Owing to the excellent promotion effect of Ni$_2$P that was found in methanol oxidation, we extended the catalyst system of Pt or Pd modified by Ni$_2$P in direct ethanol fuel cells. The Ni$_2$P-promoted catalysts were compared to commercial catalysts as well as to reference catalysts promoted with only Ni or only P. Among the studied catalysts, Pt/C and Pd/C modified by Ni$_2$P (30 wt%) showed both the highest activity and stability. Upon integration into the anode of a homemade direct ethanol fuel cell, the Pt-Ni$_2$P/C-30% catalyst showed a maximum power density of 21 mW cm^{-2}, which is approximately two times higher than that of a commercial Pt/C catalyst. The Pd-Ni$_2$P/C-30% catalyst exhibited a maximum power density of 90 mW cm^{-2}. This is approximately 1.5 times higher than that of a commercial Pd/C catalyst. The discharge stability on both two catalysts was also greatly improved over a 12 h discharge operation.

Introduction

Following the development of direct ethanol fuel cells (DEFCs), considerable attention has been directed to the electrooxidation of ethanol.[1] DEFCs are promising fuel cells that can be classified according to the membrane used, namely, proton-exchange membrane DEFCs and anion-exchange membrane DEFCs.[2] However, the commercial application of DEFCs is currently hindered by low catalytic activity and durability in the ethanol oxidation reaction.[3] Consequently, efforts are presently devoted to the development of anode materials with enhanced activity and durability for DEFCs under acidic or basic conditions.[1c, 2a, 4]

It is generally accepted that the ethanol oxidation reaction undergoes both parallel and consecutive paths, which results in various adsorbed intermediates and byproducts. Most importantly, the complete oxidation of ethanol to CO$_2$ requires cleavage of the C—C bond, which is difficult at low temperatures. Currently, platinum supported on carbon (Pt/C) is the preferred material for the dissociative adsorption of small or-ganic molecules at low temperatures in acidic solutions, whereas PtRu/C and PtSn/C alloys have been measured to be the most effective catalysts for the ethanol oxidation reaction.[5] For example, compared with a commercial PtSn/C E-TEK catalyst, the performance of a DEFC was improved if Pt$_3$Sn/C was used as the anode catalyst.[6]

Although Pd catalysts, relative to Pt-based catalysts, are nearly inert for the ethanol oxidation reaction in acidic media, these catalysts have demonstrated competitive and enhanced activity in high pH media.[1d, 7] Xu et al.[7a] compared the ethanol oxidation activity on Pt and Pd in alkaline media by cyclic voltammetry with catalysts supported on Vulcan carbon and carbon microspheres, respectively. The onset potential for ethanol oxidation on Pd shifted to lower potentials with respect to that on Pt. The peak current density for Pd was, furthermore, found to be higher than that on Pt. These results suggest that the activity for ethanol oxidation is higher on Pd than on Pt, regardless of the type of support used.

One route to develop catalysts with enhanced performance is to add a cheap metal or metal oxide promoter to the noble metal catalysts. However, one challenge is the instability of such promoters under the operating conditions, which often leads to rapid decay of catalytic performance.[8]

Recently, we found that Ni$_2$P is an effective co-catalyst that greatly promotes the activity of Pt and Pd catalysts in the oxidation of small organic molecules in fuel cells.[9] Specifically, the activity and stability of the Pt catalysts were greatly improved in the presence of Ni$_2$P in direct methanol fuel cells.[9b] Owing to the impressive promotion effect, we tried to extend the work to ethanol oxidation in direct ethanol fuel cells. Compared with the fuels of methanol and formic acid, although similarities existit is still a challenge to develop robust catalysts, because of the complicated molecular structure[10] that requires

[a] G. Li,+ J. Chang, Prof. Dr. C. Liu, Prof. Dr. W. Xing
State Key Laboratory of Electroanalytical Chemistry
Laboratory of Advanced Power Sources
Changchun Institute of Applied Chemistry, Chinese Academy of Sciences
Changchun 130022 (PR China)
. cn
E-mail: xingwei@ciac.ac

[b] Dr. L. Feng,+ Dr. B. Wickman, Prof. Dr. H. Grönbeck
Competence Centre for Catalysis
Department of Applied Physics, Chalmers University of Technology
41 296 Göteborg (Sweden)
E-mail: ligang.feng@chalmers.se
           fenglg11@gmail.com

[+] These authors contributed equally to this work.

Supporting Information for this article is available on the WWW under
http://dx.doi.org/10.1002/cssc.201402705.

more active and effective catalytic materials. In the present work, we thoroughly evaluated the effect of adding Ni_2P to a catalyst system for the electrooxidation of ethanol. In particular, the Pt-Ni_2P/C hybrid catalyst was evaluated for the electrooxidation of ethanol in acid solution, and the Pd-Ni_2P/C hybrid catalyst was evaluated for the same reaction in alkaline solution. To our delight, both Ni_2P-modified catalysts showed a remarkable enhancement in performance for ethanol oxidation. Moreover, if the hybrid catalysts were integrated into the anode of the DEFCs, both of the Ni_2P-modified catalysts showed remarkably high power density and discharge ability relative to that displayed by commercial and homemade Pt/C and Pd/C reference catalysts.

Results and Discussion

Typical transmission electron microscopy (TEM) images of the Ni_2P/C-30%, Pt-Ni_2P/C-30%, and Pd-Ni_2/C-30% catalysts are shown in Figure 1. The Ni_2P particles are uniformly distributed on the carbon surface (Figure 1a), and the lattice fringes of the Ni_2P nanoparticles are clearly observed (Figure 1b). The Pt and Pd nanoparticles are also uniformly distributed on the Ni_2P/C

Figure 1. Low-resolution and high-resolution TEM images of a, b) Ni_2P/C-30%, c, d) Pt-Ni_2P/C-30%, and e, f) Pd-Ni_2P/C-30%. Scale bars: a) 10 nm, c, e) 20 nm, and b, d and f) 5 nm.

hybrid support (Figure 1c, e), and the lattice fringes of Pt (Figure 1d) and Pd (Figure 1f) are visible. The average particle size for all the Pt catalysts is approximately 2.6 nm, and for all the Pd catalyst it is approximately 3.7 nm; both are within the range of the optimal particle sizes for fuel cells (Table S1, Supporting Information). Figure 2 shows the X-ray diffraction (XRD)
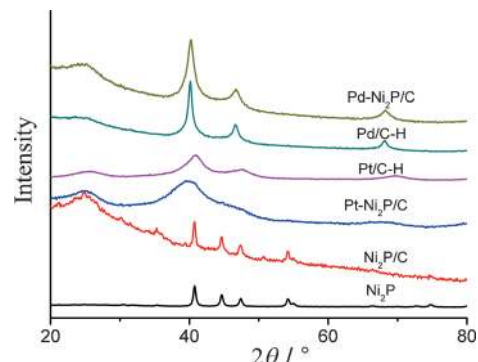

Figure 2. XRD patterns of the Ni_2P, Ni_2P/C, Pt-Ni_2P/C, Pd-Ni_2P/C (30%), Pt/C-H, and Pd/C-H catalysts.

patterns of Ni_2P/C, Pt-Ni_2P/C-30%, and Pd-Ni_2/C-30% as well as that of the homemade Pt/C and Pd/C catalysts (Pt/C-H and Pd/C-H). The peak at approximately 25° in all the samples is ascribed to carbon. Typical peaks above 30° observed on the Pt- and Pd-based catalysts are attributed to the face-centered cubic phases of Pt and Pd. The peaks for Ni_2P are not observed in the Pt-Ni_2P/C-30% and Pd-Ni_2P/C-30% catalysts, which may be covered up by the strong and broaden peaks of Pt and Pd. However, the presence of Ni_2P was further confirmed by energy-dispersive X-ray spectroscopy (EDS) and elemental distribution maps.[9]

The electrochemical surface areas of the Pt and Pd catalysts were calculated according to either the hydrogen adsorption peaks or the preadsorbed CO oxidation peaks (Table S1). Typical Pt and Pd electrochemical behavior for all the catalysts was observed (Figure S1), and CO stripping voltammetry was also used as a tool to compare the antipoisoning ability of the adsorbed intermediates (Figure S2). The results indicate that the CO tolerance of the Ni_2P-modified Pt and Pd catalysts was improved relative to that of the reference catalysts (Table S1). In the following, we will discuss the electrochemical measurements in two parts, namely, the Pt-based catalyst system in acid solution and the Pd-based catalyst system in alkaline solution.

The activities of different Pt catalysts with different loadings of Ni_2P for ethanol oxidation were compared (Figure 3a for mass activity and Figure S3a for specific activity). It is evident that the loading of Ni_2P has a pronounced effect on the catalytic performance. The optimal catalyst has a Ni_2P loading of 30% on carbon and shows a peak current of approximately 15 A m^{-2} or 1200 mA mg^{-1}_Pt. This catalyst was compared to other reference catalysts including Ni- and P-promoted Pt/C, commercial Pt/C (Johnson Matthey Co., Pt/C-JM), and homemade Pt/C catalysts (Figure 3b for mass activity and Fig-
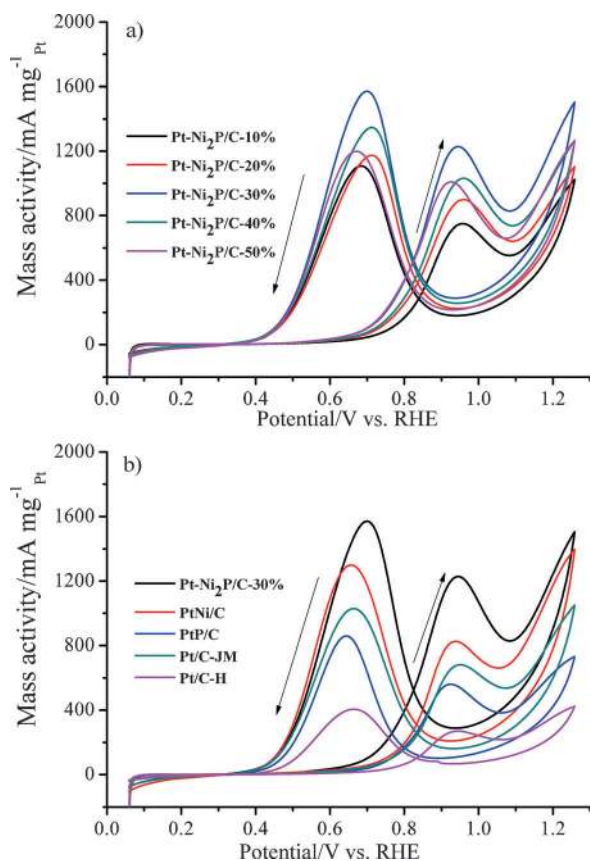
Figure 3. a) Cyclic voltammograms of Pt-Ni$_2$P/C catalysts with various loadings of Ni$_2$P in H$_2$SO$_4$ (0.5 M) containing C$_2$H$_5$OH (1 M). b) Cyclic voltammograms of the Pt-Ni$_2$P/C-30%, PtNi/C, PtP/C, Pt/C-JM, and Pt/C-H catalysts in H$_2$SO$_4$ (0.5 M) containing C$_2$H$_5$OH (1 M). Scan rate: 50 mV s^{-1}.

The stability of the promoted Pt system was compared to that of the commercial Pt catalyst over 1000 cycles (Figure S4). The Pt-Ni$_2$P/C-30% catalyst retained 60% of its initial current density, whereas the Pt/C-JM catalyst retained 45% of its initial activity. From the chronoamperometry curves (Figure S5), the Ni$_2$P-modified Pt/C catalyst also exhibited stability that was improved relative to that of various reference catalysts.

The cyclic voltammetry (CV) curve of the Pt-Ni$_2$P/C-30% catalyst at different scan rates in 0.5 M H$_2$SO$_4$/1 M ethanol is shown in Figure 4, and the curves of other Pt-based catalysts are com-
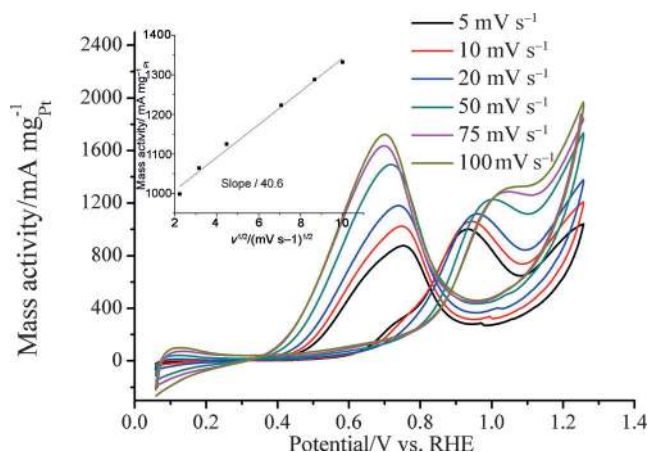

Figure 4. Cyclic voltammograms of the Pt-Ni$_2$P/C-30% catalyst at scan rates of 5, 10, 20, 50, 75, and 100 mV s^{-1}. Inset: Peak current versus the square root of the scan rate.

ure S3 b for specific activity; Table S2 a for overall peak current comparison). The peak current is approximately 2 times higher than that of the commercial Pt/C catalyst and 4.6 times higher than that of the homemade Pt/C catalyst. Moreover, it also has a larger promotion effect than the Ni- and P-promoted Pt/C catalysts (PtNi/C and PtP/C), which again confirms the promotion effect of Ni$_2$P on Pt catalyst in the oxidation of small organic molecules. Owing to the position shift of the peak current, the current at 0.9 V is also compared in Table S2 a; the trend follows the same order as the peak current. We further explored the catalytic ability of the Pt-Ni$_2$P/C-30% and Pt/C catalysts for the electrooxidation of ethanol oxidation intermediates such as acetaldehyde and acetic acid (Figure S3 c). Ni$_2$P alone had almost no catalytic activity for the oxidation of ethanol, acetaldehyde, or acetic acid, but the Pt-Ni$_2$P/C catalyst exhibited much better activity than the Pt/C catalyst for the oxidation of the same molecules. Specifically, the activity of the Pt-Ni$_2$P/C catalyst for ethanol oxidation was approximately 4.6 times higher than that of the Pt/C catalyst; however, slightly better performance was observed for the oxidation of acetaldehyde and acetic acid. The combination of Pt and Ni$_2$P indeed promoted the oxidation of small organic molecules. However, as a result of the complicated oxidation process, spectroscopic studies are needed to understand the catalytic mechanism.

pared in Figure S6. With an increase in the scan rate, the peak current increased, and this occurred along with a positive shift in the peak potential as a result of the ohmic drop generated at high current density.[11] A linear curve is observed by plotting the peak current versus the square root of the scan rate (inset in Figure 4 and Figure S6), which is indicative of a diffusion-controlled process.[12] The relationship between the peak current and the scan rates follows an equation for which the slope is related to the electron-transfer coefficient in the rate-determining step;[12, 13] in this study, the Ni$_2$P-modified Pt catalyst showed a slope that was greater than that of the reference catalyst, and the largest slope was observed for the Pt-Ni$_2$P/C-30% catalyst, which is indicative of the largest electron-transfer rate in the rate-determining step. The Tafel slope is usually used as an indication of the electron-transfer coefficient, and the lowest Tafel slope was observed for the Pt-Ni$_2$P/C-30% catalyst, which is indicative of the fastest kinetics for the catalyzed oxidation of ethanol (Figure S7).

Electrochemical impedance spectroscopy (EIS) is a useful technology to evaluate the kinetics for ethanol oxidation at different potentials. Nyquist plots for Pt-Ni$_2$P/C-30% are shown in Figure 5 a, and those for other catalysts are shown in Figure S8. The behavior of the Pt-based catalysts for ethanol oxidation was similar to that for methanol oxidation.[9b] In agreement with the CV data, ethanol oxidation started at 0.56 V, at which point a circle arc began to form. At 0.56–0.66 V, "pseudoinduc-
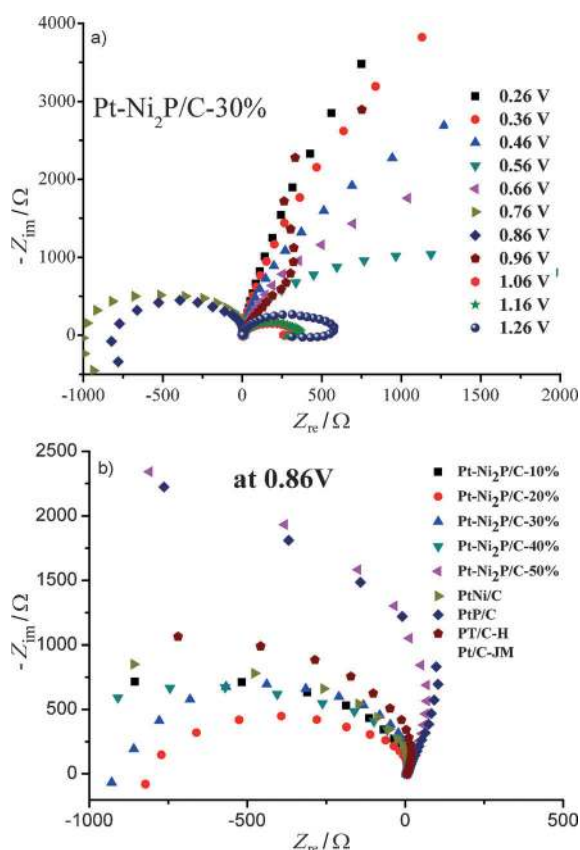
Figure 5. a) Nyquist plots of the Pt-Ni$_2$P/C-30% catalyst in the electrochemical oxidation of ethanol at different potentials. b) Nyquist plots of various Pt-based catalysts for ethanol oxidation at 0.86 V.

Figure 6. a) Cyclic voltammograms of Pd-Ni$_2$P/C catalysts with various loadings of Ni$_2$P in KOH (0.5 M) containing C$_2$H$_5$OH (1 M). b) Cyclic voltammograms of the Pd-Ni$_2$P/C-30%, PdNi/C, PdP/C, Pd/C-JM, and Pd/C-H catalysts in KOH (0.5 M) containing C$_2$H$_5$OH (1 M). Scan rate: 50 mV s^{-1}

tive" behavior was observed, for which a positive loop at high frequencies was accompanied by a low frequency loop in the fourth quadrant. This is common behavior for the Pt-catalyzed oxidation of small molecules, and it indicates that reaction intermediates such as CO are adsorbed on the Pt surface. With an increase in the potential to 0.76 and 0.86 V, because of the oxidation of the adsorbed intermediates, the shapes of the Nyquist plots changed dramatically, and the plots are located in the second and third quadrants. With a further increase in the potential, the shape of the Nyquist plots with "pseudoinductive" behavior was observed again (0.96 to 1.26 V), whereas the charge-transfer resistance was reduced because of the easily catalyzed oxidation of ethanol at high potential. Furthermore, the Nyquist plot at 0.86 V was compared for the various catalysts (Figure 5 b). According to the diameter of the semicircle or the arc that is related to the charge-transfer resistance, the Pt-Ni$_2$P/C-30% catalyst showed the smallest diameter. Thus, it has the highest activity for ethanol oxidation.

Also, the Pd-Ni$_2$P/C hybrid catalyst was evaluated, and its behavior was compared to that of various reference catalysts for ethanol oxidation under alkaline conditions. Figure 6 a compares the activity of Pd-Ni$_2$P/C catalysts with different loadings of Ni$_2$P for ethanol oxidation (Figure S9 a for specific activity). It is evident that the amount of Ni$_2$P also has a strong influence on the activity of Pd, and also in this case, the optimal loading
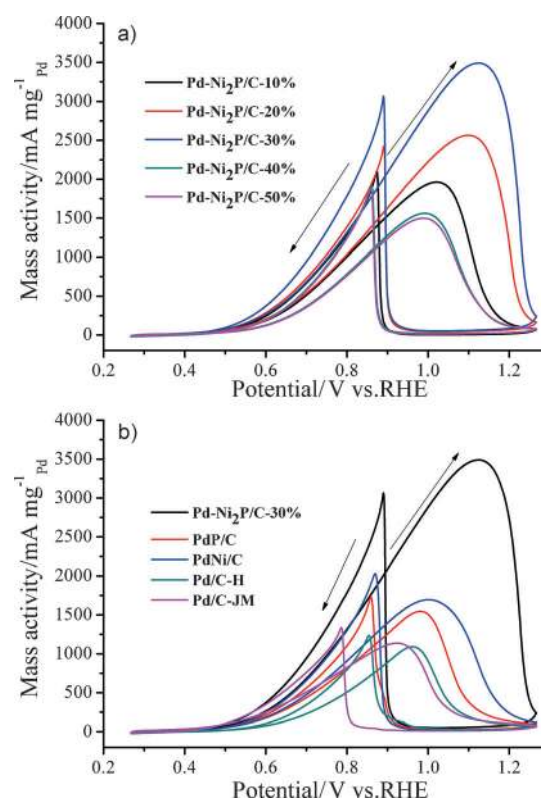
was also found to be 30% Ni$_2$P on carbon as a result of the balanced interaction between Pd and Ni$_2$P.[9a] The Pd-Ni$_2$P/C-30% catalyst was further compared to various reference catalysts including Ni- and P-promoted Pd/C, commercial Pd/C-JM, and homemade Pd/C catalysts. According to the CV curves in Figure 6 b (Figure S9 b for the specific activity; Table S2 b for the overall peak current comparison), the highest catalytic activity was observed for the Ni$_2$P-modified catalyst. Specifically, it was roughly three times more active than the Pd/C-H and Pd/C-JM catalysts and two times more active than the PdNi/C and PdP/C catalysts. Similarly, the current at 0.9 V is compared in Table S2 b, and the trend follows the same order as the peak current. From the chronoamperometry curves, improved catalytic stability was also observed on the Ni$_2$P-modified Pd catalyst (Figure S10). Furthermore, an accelerated stability test was evaluated on all the catalysts by recording CV curves over 500 cycles (Figure S11), and the activity based on the peak current was compared to the first cycle in Figure S12. It is clear that the Ni-promoted Pd catalyst suffered serious performance decay (35%) because of the loss of Ni, whereas the performance decay was slightly better for the P-promoted Pd catalyst (60%). Notably, the activity was as high as 80% of the first cycle for all the Ni$_2$P-promoted Pd catalysts. This observation further confirms the promotion effect of Ni$_2$P.

Nyquist plots for Pd-Ni$_2$P/C-30% are shown in Figure 7 a, and those for the other catalysts are shown in Figure S13. With an
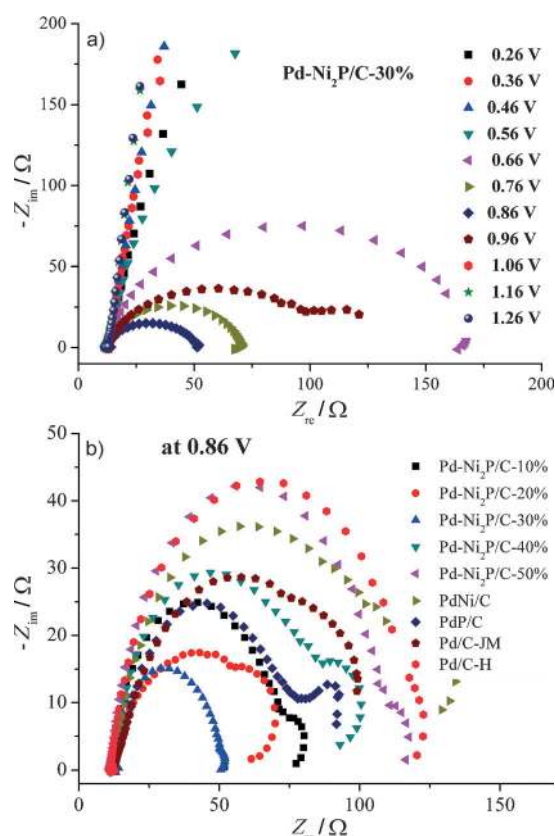
Figure 7. a) Nyquist plots for the Pd-Ni$_2$P/C-30% catalyst in the electrochemical oxidation of ethanol at different potentials. b) Nyquist plots of various Pd-based catalysts for ethanol oxidation at 0.86 V.

To evaluate the potential application of the Ni$_2$P-modified catalysts, the Pt-Ni$_2$P/C-30% and Pd-Ni$_2$P/C-30% catalysts with the analogous reference catalysts were integrated into the anode of a direct ethanol fuel cell. Figure 8a shows the steady polarization curves and power density curves for the Pt-based catalyst by using a proton-exchange membrane. The fuel cell with the Pt-Ni$_2$P/C-30% catalyst showed the highest power density of approximately 21 mW cm^{-2}, which is approximately two times higher than that of the commercial Pt/C catalyst (12 mW cm^{-2}) and the homemade Pt/C catalyst (10 mW cm^{-2}). Despite a slow performance decay upon discharging the fuel cell at 0.3 V for 12 h, the stable power density (two times higher than that of the reference catalysts) is still acceptable (Figure 8b). Figure 9a shows the steady polarization curves and power density curves for the Pd-based catalyst by using an anion-exchange membrane. The fuel cell with the Pd-Ni$_2$P/C-30% catalyst also showed the highest power density of 90 mW cm^{-2}, which is approximately 1.5 times higher than that of the commercial Pd/C catalyst (60 mW cm^{-2}) and 2 times higher than that of the homemade Pd/C catalyst (45 mW cm^{-2}). Though the performance is slightly lower than that obtained by employing the commercial anion-exchange membrane, a great promotion effect is clearly observed.[15] Upon discharging at 0.35 V, the cell with the Pd-Ni$_2$P/C anode catalyst not only showed the highest power density but it also
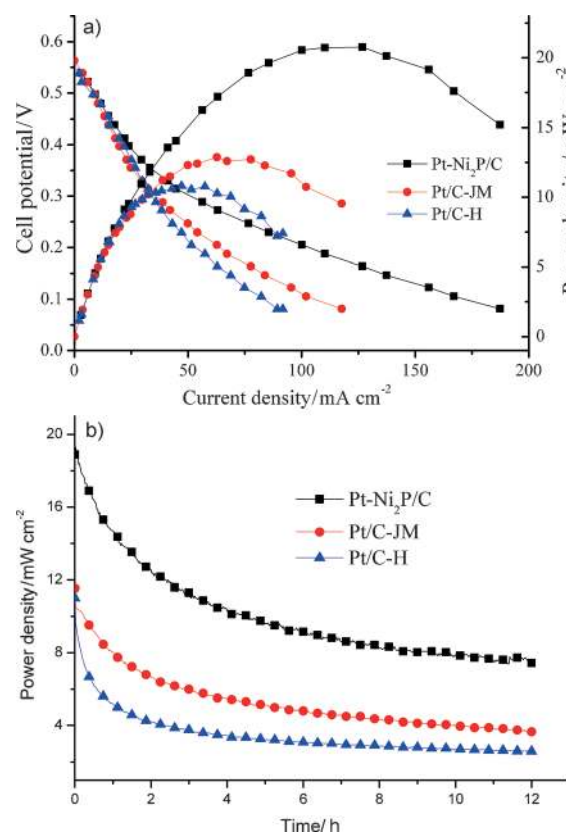
increase in the potential to 0.56 V, the shape of the plots changed from a straight line to an arc; this is consistent with the CV behavior, which is indicative of increased kinetics for ethanol oxidation. At 0.66 to 0.86 V, the shape of the Nyquist plots changed to a semicircle; this is related to charge-transfer resistance. The smallest diameter appeared at 0.86 V, and this is indicative of the smallest charge-transfer resistance and the highest kinetics for ethanol oxidation. With a further increase in the potential (0.96–1.06 V), increased resistance was observed as a result of passivation and poisoning of the Pd active sites. The Nyquist plots at 0.86 V are compared for various catalysts in Figure 7b, and the Pd-Ni$_2$P/C-30% catalyst showed the smallest diameter, which is indicative of the highest activity for ethanol oxidation. Cyclic voltammograms at different scan rates for all catalysts are shown in Figure S14, and the inset is the corresponding slope by plotting the peak current versus the square root of the scan rates. The peak current increased as the scan rate was increased, and a linear relationship was observed owing to a surface diffusion-controlled process. It is evident that the Pd-Ni$_2$P/C-30% catalyst has the greatest slope, and this indicates that it has the fastest electron-transfer rate in the rate-determining step;[14] this was further confirmed by the smallest Tafel slope (Figure S15). Thus, by combining the above results it can be concluded that the kinetics of ethanol oxidation on the Ni$_2$P-modified Pd/C catalyst is greatly increased.

Figure 8. a) Steady-state polarization and power-density curves for fuel cells with Pt-Ni$_2$P/C-30%, Pt/C-JM, and Pt/C-H as anode catalysts. b) Discharge curves at 0.3 V for fuel cells with Pt-Ni$_2$P/C-30%, Pt/C-JM, and Pt/C-H as anode catalysts. Conditions: 2 M ethanol at 60 °C. The flowing rate of ethanol was 20 mL min^{-1} and the flowing rate of O$_2$ was 200 mL min^{-1}.
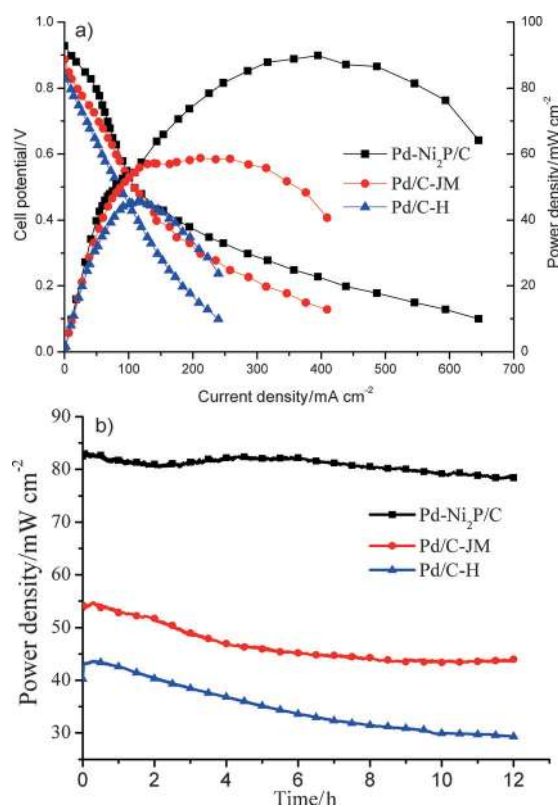
Figure 9. a) Steady-state polarization and power-density curves for fuel cells with Pd-Ni$_2$P/C-30%, Pd/C-JM, and Pd/C-H as anode catalysts. b) Discharge curves at 0.35 V for fuel cells with Pd-Ni$_2$P/C-30%, Pd/C-JM, and Pd/C-H as anode catalysts and a homemade anion-exchange membrane. Conditions: 2 M ethanol in 2 M KOH solution at 60°C. The flowing rate of ethanol was 20 mLmin^{-1} and the flowing rate of O$_2$ was 200 mLmin^{-1}.

showed the highest stability. The power density was stable at approximately 80 mWcm^{-2} (Figure 9b). Together with the electrochemical measurements, it can be concluded that Ni$_2$P is an effective catalyst promoter in combination with a noble metal catalyst in direct ethanol fuel cells. The catalytic activity and stability were remarkably enhanced relative to the values observed for the reference catalysts, including the commercial catalysts and the Ni- and P-modified catalysts. The promotion effect should be attributed to a balanced interaction between Ni$_2$P and Pd/Pt,[9] in which partial electron transfer occurs from Ni$_2$P to Pd/Pt. However, further spectroscopic and computational studies are warranted for further understanding of the catalytic mechanism.

Conclusions

Ni$_2$P as an effective catalytic promoter was evaluated in direct ethanol fuel cells. Both the Pt and Pd catalysts modified by Ni$_2$P showed greatly enhanced catalytic activity and stability for ethanol oxidation. Electrochemical impedance spectroscopy showed that the presence of Ni$_2$P in the hybrid Pt and Pd catalyst systems reduced the charge-transfer resistance. Accelerated ethanol oxidation kinetics were also observed from the small Tafel slope. Upon integration into the anode of direct ethanol fuel cells, the Pt-Ni$_2$P/C-30% catalyst showed the high-

est power density of approximately 21 mWcm^{-2} by using a proton-exchange membrane. The Pd-Ni$_2$P/C-30% catalyst also showed the highest power density of 90 mWcm^{-2} with an anion-exchange membrane. The discharge stability was also improved owing to the presence of the Ni$_2$P promoter. The promotion effect should be attributed to a balanced interaction between Ni$_2$P and Pd/Pt. The present discovery is a significant step in the development of highly active catalysts for direct ethanol fuel cells.

Experimental Section

The catalysts were prepared by a method similar to that reported in our previous publication.[9] In brief, the hybrid Ni$_2$P/C support was first prepared by solid-phase reaction with different loadings of Ni$_2$P on carbon. In the next step, Pt or Pd was deposited on the hybrid support by a microwave-assisted ethylene glycol reduction method. The amount of Ni$_2$P was varied from 10 to 50% with respect to carbon. The mass loading of Pt or Pd in the hybrid catalyst was 20%. For reference, a commercial Pt(Pd)/C catalyst together with a homemade Pt(Pd)/C catalyst and a Pt(Pd)/C catalyst modified by Ni or P were also investigated.

All X-ray diffraction (XRD) measurements were performed with a PW1700 diffractometer (Philips Co.) by using a CuK$_\alpha$ (λ = 1.5405 Å) radiation source operating at 40 kV and 40 mA. Transmission electron microscopy (TEM) and high-resolution transmission electron microscopy (HRTEM) were conducted with a TECNAI G2 instrument operating at 200 kV.

The electrochemical measurements were performed with an EG&G Par potentiostat/galvanostat (Model 273A Princeton Applied Research Co. USA) and a conventional three-electrode electrochemical cell. A Pt plate and a saturated calomel electrode (SCE) were used as the counter and reference electrodes, respectively. All the potentials were measured against the reference SCE. The working electrode was prepared by a method similar to that reported previously.[16] The apparent surface area of the glassy carbon electrode was measured to be 0.12 cm^2. All electrochemical measurements were performed in a 0.5 M H$_2$SO$_4$ or KOH solution with or without 1 M ethanol deaerated by pure nitrogen for 15 min prior to any measurements. For the electrooxidation of ethanol, the potential range was from −0.2 to +0.8 V vs. SCE in the acid solution and from −0.8 to +0.2 V vs. SCE in the alkaline solution. The CO$_{ad}$ stripping voltammograms were measured in a 0.5 M H$_2$SO$_4$ or KOH solution. CO was purged into the 0.5 M H$_2$SO$_4$ or KOH solution for 15 min to allow complete adsorption of CO onto the catalyst (the working electrode was kept at 0 or −0.6 V vs. SCE) and the excess amount of CO in the electrolyte was purged out with N$_2$ for 15 min. The amount of CO$_{ad}$ was evaluated by integration of the CO$_{ad}$ stripping peak. EIS was recorded in the frequency range from 100 kHz to 0.01 Hz with 10 points per decade. The amplitude of the sinusoidal potential signal was 5 mV. The potentials measured versus SCE were rescaled to the reversible hydrogen electrode (RHE) scale according to the Nernst equation [Eq. (1)]:

$$E_{RHE} = E_{SCE} + 0.242 + 0.059 \, pH \tag{1}$$

For the Pt-based catalysts for ethanol oxidation, Nafion 117 (DuPont) was used as the proton-exchange membrane, and pretreatment of the Nafion membrane was accomplished by successively treating the membrane with 5 wt% H$_2$O$_2$ solution at 80°C,

distilled water at 80 °C, 8 wt % H₂SO₄ solution at 80 °C, and then distilled water at 80 °C again for 30 min in each step.

Membrane electrode assemblies (MEAs) with a 9 cm² active cell area were fabricated by using a "direct paint" technique to apply the catalyst layer. The "catalyst inks" were prepared by dispersing the catalyst nanoparticles into appropriate amounts of Millipore water and a 5 % recast Nafion solution. Anode and cathode "catalyst inks" were directly painted onto carbon paper (TGPH060, 20 wt % polytetrafluoroethylene, Toray). The cathode consisted of unsupported platinum black nanoparticles (27 m² g⁻¹, Johnson Matthey) at a standard loading of 4 mg cm⁻². The anode consisted of carbon-supported Pt catalysts. A single cell test fixture consisted of machined graphite flow fields with direct liquid feeds and gold-plated copper plates to avoid corrosion (Fuel Cell Technologies, Inc.). Hot-pressing was conducted at 140 °C and 1.01 MPa for 90 s. Three different anode catalysts were investigated in this study: 20 wt % Pt on Ni₂P@Vulcan XC-72 (Pt-Ni₂P/C-30 %), 20 wt % commercial Pt/C (Pt/C-JM), and 20 wt % Pt on Vulcan XC-72 (Pt/C-H). The anode catalyst loading of Pt/C was 5 mg cm⁻², including the mass of the carbon supports.

The MEA was fitted between two graphite plates in a punctual flow bed. The polarization curves were obtained by using a Fuel Cell Test System (Arbin Instrument Corp.) under the operation conditions of 60 °C. High-purity O₂ (99.99 %) was applied as the oxidant at 200 mL min⁻¹ as the cathode atmosphere and 2 M ethanol was used as the reactant feed at the anode side at 20 mL min⁻¹. The potential range was from the open-circuit potential to 0.1 V, and one point was collected every 0.05 V; a delay of 1 min was applied to obtain steady-state plots. Both sides were under ambient pressure.

For the Pd-based catalysts for ethanol oxidation in alkaline solution, a self-cross-linked alkaline solid polymer electrolyte (xQAPS)[17] was used to prepare the anion-exchange membrane with a thickness of approximately 40 μm for the alkaline direct ethanol fuel cells tested in this study. Before fabrication of the MEA, the membrane was soaked in 2 M KOH for at least 1 week to exchange the ions to HO⁻. The membrane was then rinsed and stored in Millipore water for 2 days before later use. The cathode consisted of unsupported platinum black nanoparticles (27 m² g⁻¹, Johnson Matthey) at a standard loading of 4 mg cm⁻². The anode consisted of carbon-supported Pd catalysts. The anode, cathode, and membrane were sandwiched together and pressed at 130 kg cm⁻² for 5 min at room temperature.[18] Three different anode catalysts were investigated in this study: 20 wt % Pd on Ni₂P@Vulcan XC-72 (Pd-Ni₂P/C-30 %), 20 wt % commercial Pd/C (Pd/C-JM), and 20 wt % Pd on Vulcan XC-72 (Pd/C-H). The anode catalyst loading of Pd/C was 5 mg cm⁻², including the mass of the carbon supports. High-purity O₂ (99.99 %) was used as the oxidant at 200 mL min⁻¹ as the cathode atmosphere and the fuel used was 2 M ethanol in 2 M KOH at an operation temperature of 60 °C. The potential range was from the open-circuit potential to 0.1 V, and one point was collected every 0.05 V; a delay of 1 min was applied to obtain steady-state plots. Both sides were under ambient pressure.

Acknowledgements

[1] a) C. Bianchini, P. K. Shen, *Chem. Rev.* **2009**, *109*, 4183–4206; b) M. Z. F. Kamarudin, S. K. Kamarudin, M. S. Masdar, W. R. W. Daud, *Int. J. Hydrogen Energy* **2013**, *38*, 9438–9453; c) W. Zhou, Z. Zhou, S. Song, W. Li, G. Sun, P. Tsiakaras, Q. Xin, *Appl. Catal. B* **2003**, *46*, 273–285; d) E. Antolini, *Energy Environ. Sci.* **2009**, *2*, 915; e) L. Yang, S. Kinoshita, T. Yamada, S. Kanda, H. Kitagawa, M. Tokunaga, T. Ishimoto, T. Ogura, R. Nagumo, A. Miyamoto, M. Koyama, *Angew. Chem. Int. Ed.* **2010**, *49*, 5348–5351; *Angew. Chem.* **2010**, *122*, 5476–5479.

[2] a) W. J. Zhou, B. Zhou, W. Z. Li, Z. H. Zhou, S. Q. Song, G. Q. Sun, Q. Xin, S. Douvartzides, M. Goula, P. Tsiakaras, *J. Power Sources* **2004**, *126*, 16–22; b) R. K. Pandey, V. Lakshminarayanan, *J. Phys. Chem. C* **2009**, *113*, 21596–21603.

[3] a) J. Datta, A. Dutta, S. Mukherjee, *J. Phys. Chem. C* **2011**, *115*, 15324–15334; b) F. a. Ksar, L. Ramos, B. Keita, L. Nadjo, P. Beaunier, H. Remita, *Chem. Mater.* **2009**, *21*, 3677–3683; c) G. Cui, S. Song, P. K. Shen, A. Kowal, C. Bianchini, *J. Phys. Chem. C* **2009**, *113*, 15639–15642.

[4] a) Z.-Y. Zhou, Z.-Z. Huang, D.-J. Chen, Q. Wang, N. Tian, S.-G. Sun, *Angew. Chem. Int. Ed.* **2010**, *49*, 411–414; *Angew. Chem.* **2010**, *122*, 421–424; b) K. Tadanaga, Y. Furukawa, A. Hayashi, M. Tatsumisago, *Adv. Mater.* **2010**, *22*, 4401–4404.

[5] a) L. Jiang, L. Colmenares, Z. Jusys, G. Q. Sun, R. J. Behm, *Electrochim. Acta* **2007**, *53*, 377–389; b) J. Melke, A. Schoekel, D. Dixon, C. Cremers, D. E. Ramaker, C. Roth, *J. Phys. Chem. C* **2010**, *114*, 5914–5925; c) T. S. Almeida, L. M. Palma, P. H. Leonello, C. Morais, K. B. Kokoh, A. R. De Andrade, *J. Power Sources* **2012**, *215*, 53–62; d) M. Huang, G. Dong, N. Wang, J. Xu, L. Guan, *Energy Environ. Sci.* **2011**, *4*, 4513–4516; e) C. Lamy, S. Rousseau, E. M. Belgsir, C. Coutanceau, J. M. Leger in *54th Annual ISE Meeting*, Sao Pedro, Brazil, **2003**, pp. 3901–3908.

[6] R. F. B. De Souza, L. S. Parreira, D. C. Rascio, J. C. M. Silva, E. Teixeira-Neto, M. L. Calegaro, E. V. Spinace, A. O. Neto, M. C. Santos, *J. Power Sources* **2010**, *195*, 1589–1593.

[7] a) C. Xu, P. k. Shen, Y. Liu, *J. Power Sources* **2007**, *164*, 527–531; b) N. Tian, Z.-Y. Zhou, N.-F. Yu, L.-Y. Wang, S.-G. Sun, *J. Am. Chem. Soc.* **2010**, *132*, 7580–7581; c) C. W. Xu, H. Wang, P. K. Shen, S. P. Jiang, *Adv. Mater.* **2007**, *19*, 4256–4259; d) C. Zhu, S. Guo, S. Dong, *Adv. Mater.* **2012**, *24*, 2326–2331; e) H. Wu, H. Li, Y. Zhai, X. Xu, Y. Jin, *Adv. Mater.* **2012**, *24*, 1594–1597.

[8] a) B. Liu, J. H. Chen, X. X. Zhong, K. Z. Cui, H. H. Zhou, Y. F. Kuang, *J. Colloid Interface Sci.* **2007**, *307*, 139–144; b) M. M. Tusi, N. S. O. Polanco, S. G. da Silva, E. V. Spinacé, A. O. Neto, *Electrochem. Commun.* **2011**, *13*, 143–146; c) T. Ramulifho, K. I. Ozoemena, R. M. Modibedi, C. J. Jafta, M. K. Mathe, *Electrochim. Acta* **2012**, *59*, 310–320; d) J. C. M. Silva, R. F. B. De Souza, L. S. Parreira, E. T. Neto, M. L. Calegaro, M. C. Santos, *Appl. Catal. B* **2010**, *99*, 265–271; e) X. Zhang, H. Zhu, Z. Guo, Y. Wei, F. Wang, *Int. J. Hydrogen Energy* **2010**, *35*, 8841–8847.

[9] a) J. Chang, L. Feng, C. Liu, W. Xing, X. Hu, *Angew. Chem. Int. Ed.* **2014**, *53*, 122–126; *Angew. Chem.* **2014**, *126*, 126–130; b) J. Chang, L. Feng, C. Liu, W. Xing, X. Hu, *Energy Environ. Sci.* **2014**, *7*, 1628–1632.

[10] a) L. Calvillo, V. Celorrio, R. Moliner, A. B. Garcia, I. Camean, M. J. Lazaro, *Electrochim. Acta* **2013**, *102*, 19–27; b) L. Dong, R. R. S. Gari, Z. Li, M. M. Craig, S. Hou, *Carbon* **2010**, *48*, 781–787; c) L. Feng, Q. Lv, X. Sun, S. Yao, C. Liu, W. Xing, *J. Electroanal. Chem.* **2012**, *664*, 14–19.

[11] a) C. Amatore, C. Lefrou, F. Pflüger, *J. Electroanal. Chem. Interfacial Electrochem.* **1989**, *270*, 43–59; b) O. Antoine, Y. Bultel, R. Durand, P. Ozil,

Electrochim. Acta **1998**, *43*, 3681–3691; c) C. Amatore, E. Maisonhaute, G. Simonneau, *J. Electroanal. Chem.* **2000**, *486*, 141–155.

[12] L. Feng, X. Zhao, J. Yang, W. Xing, C. Liu, *Catal. Commun.* **2011**, *14*, 10–14.

[13] Z. Nie, C. A. Nijhuis, J. Gong, X. Chen, A. Kumachev, A. W. Martinez, M. Narovlyansky, G. M. Whitesides, *Lab on a Chip* **2010**, *10*, 477–483.

[14] a) Y. Wang, B. Wu, Y. Gao, Y. Tang, T. Lu, W. Xing, C. Liu, *J. Power Sources* **2009**,*192*, 372–375.; b) B. Xiong, Y. Zhou, Y. Zhao, J. Wang, X. Chen, R. O'Hayre, Z. Shao, *Carbon* **2013**, *52*, 181–192.

[15] a) V. Bambagioni, C. Bianchini, Y. Chen, J. Filippi, P. Fornasiero, M. Innocenti, A. Lavacchi, A. Marchionni, W. Oberhauser, F. Vizza, *ChemSusChem* **2012**, *5*, 1266–1273; b) S. Y. Shen, T. S. Zhao, J. B. Xu, Y. S. Li, *J. Power Sources* **2010**, *195*, 1001–1006.

[16] L. Feng, X. Sun, C. Liu, W. Xing, *Chem. Commun.* **2012**, *48*, 419–421.

[17] J. Pan, Y. Li, L. Zhuang, J. Lu, *Chem. Commun.* **2010**, *46*, 8597–8599.

[18] X. Sun, Y. Zhang, P. Song, J. Pan, L. Zhuang, W. Xu, W. Xing, *ACS Catal.* **2013**, *3*, 1726–1729.